Measurement of the $^{12}C(^{12}C, p)^{23}Na$ cross section near the Gamow energy

J. Zickefoose,[1,*] A. Di Leva,[2,3] F. Strieder,[4] L. Gialanella,[5,3] G. Imbriani,[2,3] N. De Cesare,[5,3,†] C. Rolfs,[6] J. Schweitzer,[1] T. Spillane,[1] O. Straniero,[7,8] and F. Terrasi[5,3]

[1]*Department of Physics, University of Connecticut, Storrs, Connecticut 06269, USA*
[2]*Department of Physics "E. Pancini," University of Naples "Federico II," Naples, Italy*
[3]*INFN Section of Naples, Naples, Italy*
[4]*Department of Physics, South Dakota School of Mines and Technology, Rapid City, South Dakota 57701, USA*
[5]*Department of Mathematics and Physics, Università della Campania L. Vanvitelli, Caserta, Italy*
[6]*Fakultät für Physik und Astronomie, Ruhr-Universität Bochum, Germany*
[7]*INAF, Osservatorio astronomico di Teramo, Italy*
[8]*INFN, Laboratori Nazionali del Gran Sasso, Assergi, Italy*

(Received 22 November 2017; published 26 June 2018)

The fusion reaction $^{12}C(^{12}C,p)^{23}Na$ has been studied from $E = 2.00$ to 4.00 MeV by particle spectroscopy. The data reveal broad resonances above $E = 3.00$ MeV and are compatible with previously reported resonance structure around $E = 2.1$ MeV. The data were limited at low energies by low count rates as well as possible background contributions. This experiment extends the previously achieved low-energy measurement by charged particle spectroscopy to 2 MeV, which corresponds to the high-energy side of the astrophysically relevant temperature. Present knowledge of level structures and nonresonant contribution cannot explain the results of the present experiment, which may change the $^{12}C + {}^{12}C$ reaction rate significantly. Despite the progress decreasing the low-energy limit, any extrapolation into the astrophysical energy range remains highly uncertain based on available experimental data.

DOI: 10.1103/PhysRevC.97.065806

I. INTRODUCTION

Carbon burning marks the ignition of the third nuclear fuel supply after hydrogen and helium burning in the evolution of massive stars, i.e., $M > 8M_{\odot}$. As helium is exhausted in the interior of these stars the ashes, carbon and oxygen, build up in the stellar core. In the case where the central temperature becomes sufficiently high, the next phase proceeds primarily through burning of carbon because the Coulomb barrier is lowest for the carbon fusion reactions $^{12}C(^{12}C,\alpha)^{20}Ne$ (Q = 4.62 MeV) and $^{12}C(^{12}C, p)^{23}Na$ (Q = 2.24 MeV) [1–3]. Therefore, these reactions represent some of the most important processes in late stellar evolution. The stellar reaction rates of carbon burning determine the properties of massive stars during the most advanced phases of their evolution as well as their contribution to the chemical evolution of the universe. In addition, the $^{12}C + {}^{12}C$ rate is the engine of type Ia supernovae and, in turn, affects their outcomes.

The stellar core temperature is strongly correlated with the stellar mass and a minimum mass necessary for the ignition of carbon is commonly referred to as M_{up}. This parameter determines the upper limit for carbon-oxygen white dwarf progenitors and the lower limit for core collapse supernovae [4]. Stars with masses slightly greater than M_{up} proceed, due to significant plasma neutrino cooling, through an off-center carbon ignition [5] and eventually end their lives as oxygen-neon-magnesium (ONeMg) white dwarfs. Stars with greater mass will commence core carbon burning followed by neon, oxygen, and silicon burning and die cataclysmically as iron core collapse supernovae [6]. Naturally, stars with mass less than M_{up} will never attain sufficient temperatures to burn carbon and fade away as carbon-oxygen (CO) white dwarfs. However, CO white dwarfs in closely accreting binary systems may gain enough mass from the companion to overcome the Chandrasekhar mass limit. In this case, carbon ignites at the center causing a thermonuclear runaway. These objects are believed to be type Ia supernovae progenitors [7–12]. Consequently, the expected number of CO and ONeMg white dwarfs in a given stellar population as well as the rate of type Ia supernova events depend on the $^{12}C + {}^{12}C$ reaction rates.

Stellar evolution calculations mainly using heavy-ion nuclear-reaction rates from CF88 [13] suggest that carbon burning in massive stars takes place at $T > 5 \times 10^8$ K [14,15], corresponding to a Gamow energy as low as $E_G \approx 1.5$ MeV. However, the exact ignition temperature of carbon burning, and in turn the value of M_{up}, is very sensitive to the $^{12}C + {}^{12}C$ nuclear reaction rate [16]; as the C burning temperature is lower, the minimum stellar mass required to reach ignition conditions becomes smaller. The existence of low-energy $^{12}C + {}^{12}C$ resonances at interaction energies below $E \approx 2$ MeV would substantially reduce the C burning ignition temperature [10]. Because of the potential molecular structure of the ^{24}Mg compound nucleus, the presence of such low-energy resonances has long been proposed [17]. In contrast, the fusion

*Corresponding author: jzickefoose@mirion.com
†Deceased.

TABLE I. List of possible transitions in $^{12}C(^{12}C,p)^{23}Na$. The energy E_p of the emitted proton is calculated for $E = 2.6$ MeV at $\theta_{lab} = 130^\circ$ and given in the laboratory system.

Transition	J^π	E_x (MeV)	Q_x (MeV)	E_p (MeV)
p_0	$3/2^+$	0	2.240	3.71
p_1	$5/2^+$	0.440	1.801	3.33
p_2	$7/2^+$	2.076	0.165	1.95
p_3	$1/2^+$	2.391	−0.150	1.69
p_4	$1/2^-$	2.640	−0.399	1.48
p_5	$9/2^+$	2.704	−0.463	1.43
p_6	$3/2^+$	2.982	−0.741	1.20
p_7	$3/2^-$	3.678	−1.437	0.67
p_8	$5/2^-$	3.848	−1.607	0.53
p_9	$5/2^+$	3.914	−1.673	0.48
p_{10}	$1/2^+$	4.430	−2.189	0.13

hindrance model [18] predicts a steeper drop of the $^{12}C + ^{12}C$ cross section compared to other low-energy extrapolations, e.g., Ref. [13]. A $^{12}C + ^{12}C$ cross section governed by the hinderance model would require an increased temperature to ignite C burning. Carbon burning nucleosynthesis and all subsequent evolutionary phases would be strongly affected by such variations of temperature and stellar mass, respectively. For instance, all the elements produced in the C-burning shell of massive stars, among which are the intermediate-light elements Ne, Na, Mg, and Al, are affected by a change of the temperature. In addition, the C-burning shell is a promising site for the synthesis of the s-process weak component. In this context, temperature plays a fundamental role, because of the sensitivity of the available ^{13}C, the fuel of the $^{13}C(\alpha,n)^{16}O$ neutron source, on the photodisintegration rate of ^{13}N [19].

Current estimates of carbon fusion reaction rates at astrophysically relevant energies rely on cross-sectional extrapolations from higher energies. Low-energy studies of $^{12}C + ^{12}C$ reactions have focused either on charged particle or γ-ray spectroscopy. Charged particle spectroscopy has the advantage that the total fusion cross section can in principle be measured, while γ-ray spectroscopy cannot account for direct transitions to the ground state of the residual nucleus. Furthermore, γ-ray spectroscopy has been limited at low energies due to background arising from hydrogen contamination, both ^1H and ^2H, within the target. Therefore, particle spectroscopy measurements historically reached a lower energy limit than γ-ray spectroscopy experiments. However, the condition of being a total cross-sectional measurement is not fulfilled in practice in the case of particle spectroscopy due to finite energy resolution and a low-energy detection limit. This point is supported by the data in Table I where p_0 and p_1 are left with significantly more energy after the transition than any other proton groups. The low residual energy of p_7 through p_{10} leave them either below the typical noise threshold or buried in low-energy beam-induced background. Furthermore, with the narrow separation in emitted proton energy between p_0 and p_1, the two groups may not be resolved, particularly when thick targets are used.

A number of $^{12}C + ^{12}C$ experiments [20–28] obtained useful data below the Coulomb barrier and all have observed pronounced structures in the excitation function. Recently, the hydrogen contamination problem was significantly reduced [28] to levels sufficient to reach 2.1 MeV in the center-of-mass system (all energies from this point on will be expressed in the center-of-mass energy). A particularly strong resonance was found at 2.14 MeV, enhancing the reaction rates in the stellar temperature range [28]. The collection of data required active and passive shielding but remained limited at the low-energy limit mainly by natural background. In a different approach, γ-particle coincidences have been utilized in a measurement at Argonne National Laboratory, USA [29]. The total S factor of this work is in good agreement with that of Ref. [28], but the data set consists of only a few data points and therefore does not provide any information about possible resonance structures in the energy region covered by the experiment. Furthermore, no information is provided on the calculation of the total S factor from the experimental data. Another approach using a solenoid spectrometer is also under study, and promising results at energies above 4 MeV have been published [30].

The $^{12}C + ^{12}C$ cross section $\sigma(E)$ at low energies is typically expressed in terms of the modified astrophysical S factor [20]:

$$S^* = E\sigma(E)\exp(2\pi\eta + gE) \quad (1)$$

with $\eta = 13.88E^{-1/2}$ and $g = 0.46\ \mathrm{MeV}^{-1}$, where the energy E is given in MeV.

Much of the data collected to date for the $^{12}C + ^{12}C$ reaction are shown in Fig. 1, where the low-energy limit reached by each respective experiment can be seen. Clearly there are large discrepancies between a number of the data sets, which may depend on the detection method as well as the particular strength of contamination within the target.

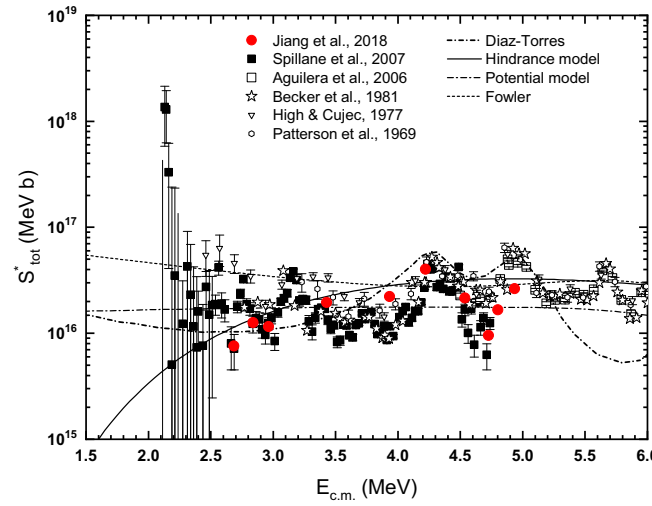

FIG. 1. The total S^* factor of the $^{12}C + ^{12}C$ reactions compared to some theoretical models, i.e., the hindrance model [18], a potential model calculation based on Ref. [31], and the recent model of Diaz-Torres [32], as well as the parametrization of Caughlan and Fowler [13].

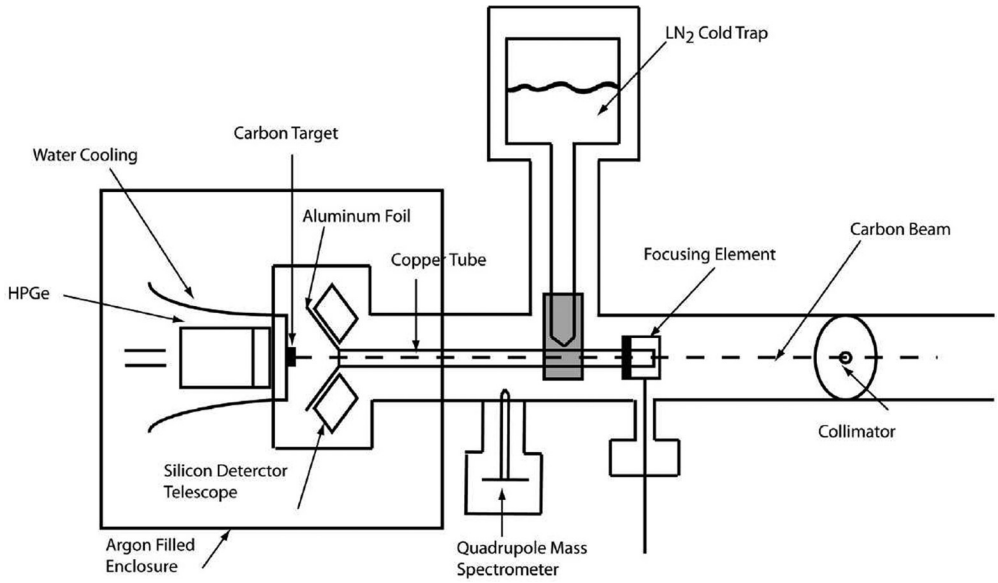

FIG. 2. Schematic of the experimental setup where the beam direction is from right to left.

The use of optical potentials to explain the resonant behavior of the $^{12}C + ^{12}C$ system [33,34] has had success in describing the energy dependence of both elastic scattering and nuclear reaction cross sections. The existence of corresponding structures in both channels has led optical models to predict the existence of a resonance at $E = 1.5$ MeV [34].

Such a resonance would significantly reduce M_{up}, would decrease the number of CO white dwarf progenitors, and may explain the origin of superburst ignition [35,36]. Presently, no model accurately predicts the observed parameters of superbursts using the reaction rates based on current cross-sectional extrapolations, while under the assumption that a resonance exists in the $^{12}C + ^{12}C$ reaction at $E = 1.5$ MeV models could account for the observations [36]. The proposed resonance with a nominal fiducial strength of $\omega\gamma = 3.4 \times 10^{-8}$ eV would dominate the reaction rates over a wide temperature range around 5×10^8 K. The verification of such a resonance should be the ultimate aim of $^{12}C + ^{12}C$ measurements at astrophysical energies.

We report on measurements of the emitted protons from the ^{23}Na channel by particle spectroscopy, i.e., to the ground state (p_0) and first excited state (p_1) of ^{23}Na. Recently, an improbable multiple scatter process involving deuterium contamination within carbon targets was identified as a source of beam-induced background in charged particle spectroscopy [37,38]. This background significantly reduces the ability to measure directly into the Gamow window but may be overcome with the proper choice of targets, e.g., highly ordered pyrolytic graphite (HOPG). The present work utilized HOPG to reduce this contribution to the background and extend the measurement down to 2.0 MeV.

II. EXPERIMENTAL TECHNIQUE

The equipment and procedures are similar to those described previously [28], with the following differences: The beam was provided by a 3-MV Pelletron accelerator, $\Delta E - E$ telescopes were used to collect protons emitted from the $^{12}C(^{12}C,p)^{23}Na$ reaction, and HOPG carbon targets were utilized.

The 3-MV Pelletron tandem at the Center for Isotopic Research on the Cultural and Environmental heritage (CIRCE), Università della Campania L. Vanvitelli, provided the ^{12}C beam with up to 15 particle μA on target. A calibration of the terminal voltage was performed using the 992-keV resonance in the $^{27}Al(p,\gamma)^{28}Si$ ($Q = 11585$ keV) reaction [39,40]. The energy calibration verified that the absolute energy and the energy spread are known within 3 and 2 keV, respectively. These uncertainties result in a negligible error of less than 0.3% for a 3- to 7-MeV ^{12}C beam.

A. Target chamber

The experimental setup (Fig. 2) was placed at the end of an accelerator mass spectrometry system including several magnetic and electric filters; it therefore provided an ion beam of high isotopic purity [41]. Beam profile monitors at several locations along the beam line were used to have nearly the same beam optics at all energies. The beam line is entirely equipped with conflat (CF) flanges with the exception of the end station, where a Viton seal ensured the electrical insulation of the target. The beam passed through a series of collimators as well as a Cu tube extending to within 4 cm from the target and was stopped at the C target.

The target was mounted on a water-cooled stainless-steel backing. Visual inspection showed that the beam spot on target had a nearly circular shape with a diameter of about 5 mm. The copper tube was connected to an electrically isolated cold trap and was biased to a voltage of -300 V for suppression of secondary electrons so that the beam current could be accurately integrated on target using the ADC of the NEC accelerator control system; a comparison with a Faraday cup reading indicated that the beam current was measured with an accuracy of 3%.

A pressure in the target chamber of 5×10^{-9} mbar was achieved with the cold trap cooled to LN_2 temperature. Additionally, before starting each series of measurements the end station was baked out, reducing, in particular, light mass contaminants in the chamber walls. Finally, since the vacuum was most likely limited by the Viton O-ring in the end station, the setup was enclosed in a sealed plastic box flushed with argon (see Fig. 2). Argon has the advantage that it is efficiently pumped and unlikely to introduce hydrogen isotopes to the rest gas. The composition of the vacuum rest gas, in particular the hydrogen content, was monitored through a quadrupole mass spectrometer connected to the target chamber.

An HPGe detector was also placed in close proximity to the target to monitor possible target contaminants interacting with the carbon beam. However, no spurious γ lines were seen in the spectrum during the experiments.

B. Detectors and electronics

Two identical $\Delta E - E$ telescopes (ΔE-Si detector: area $A = 300$ mm^2, thickness $t = 15\,\mu$m; E-Si detector: $A = 300$ mm^2, $t = 300\,\mu$m) were installed at an angle $\theta = 130^\circ$, laboratory angle, on opposite sides of the beam axis at a distance of 6 cm from the target. The detectors were cooled to 0 °C using a cryostat in order to reduce the detector leakage current and lower the electronic noise. During data analysis, only those events were considered that left a signal in both detectors of a single telescope. Using a calibrated α source, the total solid angle of the two telescopes (i.e., of the ΔE detectors) was determined to be $\Omega = 0.0159 \pm 0.0003$, consistent with the geometry.

The beam heated the target to a temperature of several hundred degrees Celsius, which could have had a significant impact on the performance of the Si detectors. Therefore, in addition to the direct cooling of the detectors, a heat shield avoided thermal damage to the detectors. This heat shield was connected to a Cu tube coupled to the cold trap, i.e., part of the electron suppression, and consisted of a thin aluminum foil (thickness 5 μm) extending between the target and the detectors. With the heat shield installed, no thermal effects were observed.

Measurements were performed in a thick-target approach; i.e., the yield is the result of the integration over a target that is infinitely thick to the incident ^{12}C beam. Because of the exponential decrease of the $^{12}C + {}^{12}C$ cross section, i.e., a factor 10 every energy step of $\Delta E = 250$ keV, the proton group p_0 to the ground state of ^{23}Na and the proton group p_1 to the first excited state at 440 keV each had a width of about 250 keV. Furthermore, the close geometry of the detectors caused a kinematic broadening of the proton groups by about 200 keV and the Al foils led to an energy loss of about 75 keV as well as an energy straggling of about 10 keV for both groups. These effects did not allow for resolution of the p_0 and p_1 groups; thus only the summed yield of both groups was available for the present studies. The α particles from the fusion reaction ^{12}C(^{12}C,α)^{20}Ne were stopped in the ΔE detectors and could not be detected due to the coincidence requirement in the telescopes.

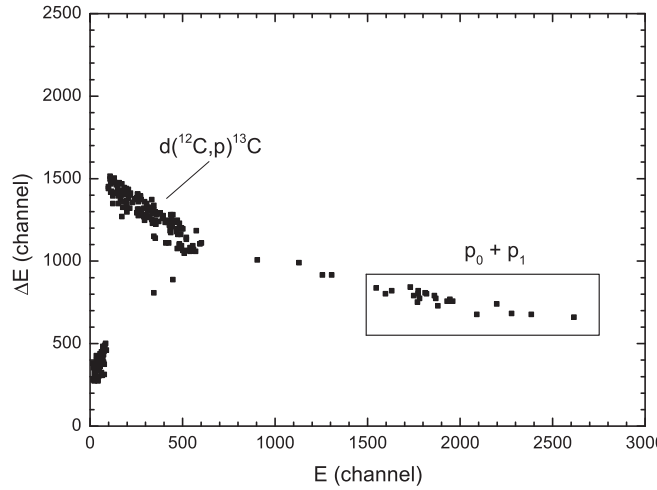

FIG. 3. A sample $\Delta E - E$ matrix taken at $E = 2.6$ MeV with the HOPG target. The region of interest for the protons from the ^{12}C(^{12}C, p)^{23}Na reaction (p_0 and p_1) is indicated and is constrained from the other proton groups by kinematics. The continuum of low-energy counts arises from the remaining deuterium contamination in the target, through the $d(^{12}C, p)^{13}C$ reaction. Ejected protons corresponding to higher excited states of the ^{23}Na nucleus (p_2, p_3, p_4, ...) are found between the region of interest of the $p_0 + p_1$ group (ROI) and the deuterium protons as well as merged with the deuterium protons.

Conventional electronics were used to store, event by event, the signals from the individual detectors of both telescopes as well as their coincidences using time-to-amplitude converters (resulting time resolution = 250 ns). Once gated properly, these conditions resulted in a $\Delta E - E$ matrix, an example of which can be seen in Fig. 3. The matrices were calibrated using a proton beam at $E = 1.0$ to 5.0 MeV that was scattered off the carbon target; the observed energy dependence of the elastically scattered protons was consistent with the calculated energy loss in the Al foil and the ΔE detector. A run without beam over 5 days showed no events in the region of interest, thus cosmic-ray events are negligible due to the coincidence requirement in the telescopes. Previous work [25] has shown that the angular distributions of the p_i groups are described at low energies by Legendre polynomials of second order, $P_2(\theta)$, where $P_2(\theta_{c.m.} = 125^\circ) = 0$, i.e., close to our detection angle of $\theta_{c.m.} \approx 136^\circ$, which is nearly constant over the energy range studied in the present experiment. Thus, we assumed that the yields for the investigated groups represent angle-integrated yields and did not consider any uncertainties due to this assumption.

C. Targets and background

A number of high-purity carbon targets were tested throughout the experiment: graphite targets with purities of 99.997, 99.98, 99.95% (obtained from Goodfellow), and 99.999% (obtained from Lesker) as well as pristine highly ordered pyrolytic graphite (HOPG) targets (obtained from Optigraph and Momentive Performance Materials). HOPG has been found [42] to exhibit very low levels of contamination from

other elements, such as a hydrogen content on the order of 0.3 ppm.

The thick target yield method applied here has the major advantage that very thick targets can be used. All targets used in the experiment had a thickness of about 1 mm. Thus, target deterioration had a negligible effect on the measured yields. This, however, comes at the price of a deconvolution required to derive the $^{12}C + {}^{12}C$ cross section (see Sec. III). Although thick carbon targets are rather heat resistant, there are other technical difficulties, e.g., effective cooling of target and detectors, radiated heat, and deposition of sputtered carbon, that result in considerable limitations if the beam intensity is significantly increased. For the available beam intensity of 15 particle μA, these effects did not hamper the measurements.

A known source of background is the reaction $d(^{12}C,p)^{13}C$, i.e., incoming ^{12}C projectiles bombarding deuteron contaminants in the target. The emitted protons from this background reaction have rather low energies and thus are well separated from $^{12}C(^{12}C,p)^{23}Na$ reaction products. However, during the course of the experiment, it was realized that deuterium contamination in standard graphite targets show, at energies below $E = 2.5$ MeV, an almost energy-independent yield distribution with an absolute value strongly depending on the target itself. Tests with an ^{16}O beam revealed that the observed yield was nearly independent of the mass of the projectile, and it was concluded that a major fraction of the yield originated from elastically scattered deuterium contaminants through the channel $d(^{12}C,d)^{12}C$ and a subsequent deuteron-induced reaction $^{12}C(d,p)^{13}C$. Because of the exchange of projectile and target nuclei with respect to the typical beam-induced background, the latter reaction takes place at a much higher center-of-mass energy and the proton ejectiles may attain an energy that traverses the ROI of the studied reaction $^{12}C(^{12}C,p)^{23}Na$. Therefore, in the detector telescope the reaction products cannot be distinguished from these background protons (see Refs. [37,38] for details) and deuterium must be significantly reduced from the target to achieve a clean measurement of the $^{12}C + {}^{12}C$ cross section.

The use of the HOPG targets and improvements in the vacuum system led to a significant reduction in the hydrogen and deuterium contaminations and thus a much higher sensitivity to the protons from the $^{12}C(^{12}C,p)^{23}Na$ reaction. The reduced deuterium content coupled with a process to account for unwanted background protons in the ROI led to an extension of the measurement down to 2 MeV.

III. DATA ANALYSIS

The reaction yield of the infinitely thick C target, $Y^{\infty}(E)$, was obtained from $E = 2.0$ to 4.0 MeV, with energy steps of $\Delta E = 20$ to 100 keV: $N_p = N_C \frac{\Omega}{4\pi} Y^{\infty}(E)$, where N_p is the number of counts for the proton groups and N_C is the number of ^{12}C projectiles on target, with an accumulated charge of about 1 Coulomb at low energies. The solid angle, Ω, includes a correction for the transformation from laboratory into center-of-mass system [43]. The proton groups p_0 and p_1 were included in the analysis while protons corresponding to higher excited states of the residual ^{23}Na nucleus cannot be distinguished from $d(^{12}C,p)^{13}C$ background at all energies. A charge of 1 Coulomb under the present experimental conditions corresponds to approximately 1 day of continuous beam time.

The present technique avoids the previous problems of target deterioration and/or carbon deposition that occur when using thin C targets, as discussed in Refs. [25,27]. The thick-target yield curve is shown in Fig. 4, where one observes the expected steep drop over the entire energy range due to the repulsive force of the Coulomb barrier. However, some structures due to resonances can be clearly identified above $E = 3.0$ MeV. Similar structures have been observed in the past as well (see S^* factor representation in Fig. 1).

Although improvements in the setup and the use of HOPG targets reduced the background contribution from deuterium significantly, small amounts were still detected. Therefore, a background correction was applied and the process is outlined here (for full details, see Ref. [38]).

The study of many targets with various levels of deuterium contamination suggested that there is a direct relation between the amount of deuterium in the target and the number of background counts in the ROI. Furthermore, some of the targets contained a sufficiently large amount of deuterium contamination that a detailed relation between the deuterium content in the target and background counts in the ROI could be established down to 2 MeV. Since the amount of hydrogen isotopes present on the surface of the target may change after exposure to the atmosphere or baking at high temperatures or as a function of integrated beam current, an *in situ* method of monitoring deuterium content of the target is desired. Fortunately, protons from the one-step $d(^{12}C,p)^{13}C$ contamination reaction are visible in the $\Delta E - E$ matrix; see Fig. 3. During the measurement, the background counts in the ROI are proportional to the counts in the low-energy region of the matrix. The number of counts in the low-energy portion of the $\Delta E - E$ matrix, which at high levels of deuterium contamination arise

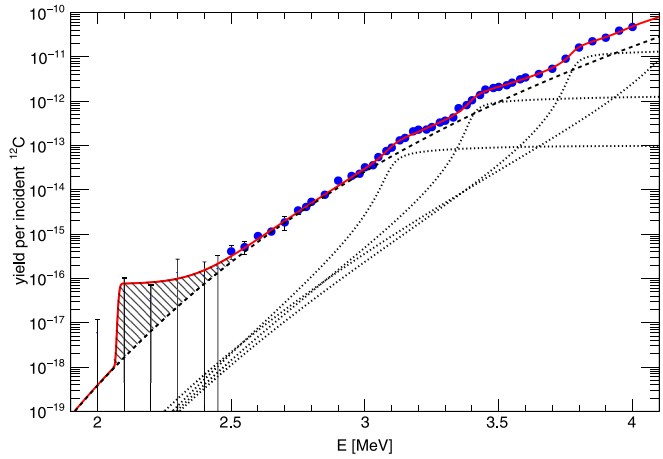

FIG. 4. Thick-target yields (blue circles) of the $^{12}C(^{12}C,p)^{23}Na$ fusion reaction as a function of the center-of-mass energy E. The (red) solid line was obtained by a fit to the data including a nonresonant component and several broad resonances. The individual contributions to the total yield are shown as dashed and dotted lines for the nonresonant contribution and the resonances, respectively. For details, see the text.

nearly entirely from the $d(^{12}C,p)^{13}C$ reaction, were mapped against the number of excess counts in the ROI. The resulting relation between the two groups was used as an empirical model to determine the appropriate background subtraction for each data point based on the number of counts in the $d(^{12}C,p)^{13}C$ reaction continuum in the $\Delta E - E$ matrix. While protons from lower energy groups may occupy the same region of the $\Delta E - E$ matrix as the one-step $d(^{12}C,p)^{13}C$ protons and there was no way to distinguish protons originating from the different mechanisms, the number of protons arising from the $d(^{12}C,p)^{13}C$ were large in comparison to those from the lower energy proton groups where the background subtraction had any significance. Through kinematics as well as branching ratios of the various proton groups, it was estimated that 5% of the protons in the deuterium region were actually lower energy proton groups from the $^{12}C(^{12}C,p)^{23}Na$ reaction at $E = 2.5$ MeV and estimated at 2% below $E = 2.25$ MeV. However, all protons in the selected region were assumed to be resulting from the $d(^{12}C,p)^{13}C$ reaction and no further estimates were made to remove the contribution from the lower energy proton groups.

The applied correction ranges between 2% and 10% at $E = 2.8$ and 2.1 MeV, respectively. Therefore, in spite of the enormous efforts to reduce the background, the two-step effect likely remains present in small quantities at low energies and might still be underestimated below 2.5 MeV. It is important to note that the lowest energy points between 2 and 2.5 MeV recorded only a few counts. These data points are shown in Fig. 4 as 90% upper limits according to a Poisson distribution and have been excluded from the fitting procedure discussed below. The poor statistics of the lowest energy point coupled with no information below that point creates a challenging environment to reliably deduce any concrete information about a potential low-energy resonance. However, the upper limits indicate evidence for the existence of some structure in the vicinity of 2.1 MeV, as observed previously [28].

In order to arrive at a thin-target yield curve, $Y(E)$, and subsequently a transformation into the cross section $\sigma(E)$, usually the thick-target yield curve is differentiated; i.e., the yield difference between two adjacent points $Y^{\infty}(E)$ and $Y^{\infty}(E - \Delta)$ is calculated. However, this procedure requires that the step size Δ is small compared to the width of any resonance structures, a requirement which is most likely not fulfilled in the $^{12}C + ^{12}C$ reactions where resonance structures exist over a broad energy range with unknown resonance widths. Therefore, in the present analysis we deconvolved the raw thick-target yield curve by fitting to the data the integral of the fusion cross section from zero to E. Thus, the reaction yield for the infinitely thick target is given by

$$Y^{\infty}(E) = \int_0^E \frac{\sigma(E)}{\epsilon(E)} dE, \tag{2}$$

where $\epsilon(E)$ is the stopping power of ^{12}C ions in graphite obtained from Ref. [44].

All observed structures were accounted for by assuming the cross section to be the sum of several isolated broad resonances. These resonances are described by individual Breit-Wigner functions including the energy dependence of the penetrabilities of entrance and exit channel [43].

The ^{24}Mg compound nucleus states are largely unknown in the energy range explored by this study. A determination of these parameters from the experimental data is impossible due to the complexity of the decay scheme, e.g., involvement of several excited states, the possible overlap of resonance structures, and the presence of a strong $^{12}C(^{12}C,\alpha)^{20}Ne$ channel. Therefore, the analysis provides only a phenomenological approach to describe the data and the fit will not deliver actual resonance parameters of the compound nucleus states. The aim of this simple approach is to translate the observed yield into a reliable S^* factor curve without taking into account the details of the nuclear structure. The applied simplifications should have only a minor influence on the shape of the extracted S^* factor. Finally, three resonances could be identified (see Figs. 4 and 5), each fit with two phenomenological partial widths and the resonance energy leading to a total of 10 fit parameters including a scaling parameter that accounts for the nonresonant contribution (see below). The energies of the three resonances are $E = 3.10$, 3.40, and 3.78 MeV, respectively. An additional high-energy resonance was required to fit the thick-target yield data above 3.8 MeV and should account for contributions from higher lying resonances. Such a resonance is not confined by the present data, and a resonance energy of $E = 4.2$ MeV as obtained from data by Becker *et al.* [25] appeared to be a reasonable choice.

In addition to the resonant cross section, a major contribution to the yield results from the nonresonant cross section. The nonresonant fraction of the yield was estimated by adding a component with a constant S^* factor, as suggested by some work utilizing Wood-Saxon potentials to fit the low-energy

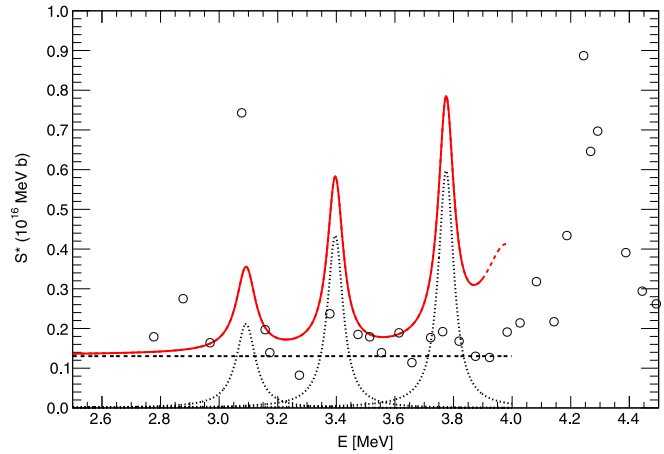

FIG. 5. The modified S^* factor for the sum of the p_0 and p_1 channels (solid line) is shown together with the corresponding data (p_0 and p_1 only) of Becker *et al.* [25] (open circles). The individual contributions for the resonances (dotted line) as well as the flat nonresonant contribution (dashed line) are also presented (for explanations, see Fig. 4). Note that a high-energy resonance at $E = 4.2$ MeV as inferred from Becker *et al.* [25] had to be included to fit the thick-target yield data above 3.8 MeV. This resonance is not confined by the present data and thus indicated by the dashed extension of the solid line.

$^{12}C + ^{12}C$ fusion cross section [45]. However, it is worthwhile to emphasize that the existing experimental data are insufficient to distinguish between existing theoretical predictions or models at low energies (see Fig. 1). Any adjustment in the nonresonant contribution to the cross section can be compensated by higher or lower amplitudes in the various resonance structures between $E = 2$ and 5 MeV. As a consequence, any extrapolation to energies below this window remains extremely difficult and probably not reliable.

IV. RESULTS

A. S* factor of p_0 and p_1 channel

With the resonant and nonresonant contributions to the cross section defined, the S^* factor for the p_0 and p_1 channels may now be computed with Eq. (1). The $p_0 + p_1$ channel S^* factor is shown in Fig. 5 as a solid line and compared to the charged particle experiments of Ref. [25]. While the present work did not measure above 4 MeV and therefore does not confine the highest energy resonance shown in the figure, the location of the next three lower energy resonances are in fair agreement with the results of Ref. [25]. However, the absolute strengths of these resonances differ significantly from the previous study [25]. This ambiguity strongly demonstrates that our knowledge of the $^{12}C + ^{12}C$ reaction cross section even at relatively moderate energies, between 3 and 4 MeV, is far from being complete and settled. Since the time of data collection, subsequent charged particle measurements have been performed in Ref. [46] and also show general agreement with the present data in the location of the structures down to 3 MeV.

The effects of electron screening [47] are negligible: With an estimated electron screening potential energy of $U_e \approx 1$ keV, the energy of the 2.1-MeV resonance is shifted by about 1 keV and the resonance yield is increased by about 2%, well below the present experimental uncertainties.

B. Low-energy resonances

A previous work [28] has observed a resonance in the vicinity of 2.1 MeV. It should be stressed that poor counting statistics, relatively large step size, and lack of data below 2 MeV make the task of quantitatively defining a potential resonance in this energy range, as seen before, very difficult. Further experiments are necessary to properly identify the presence of a resonance and more accurately define its parameters.

The upper limits for the resonance strength of such a potential low-energy resonance at approximately 2.1 MeV has been analyzed in the narrow resonance formalism [43]:

$$Y_R = \lambda^2 \frac{\omega\gamma}{\varepsilon(E_R)}, \tag{3}$$

where λ is the de Broglie wavelength, $\varepsilon(E_R)$ is the stopping power at the resonance energy E_R [44], and $\omega\gamma$ is the resonance strength. We assume a value of $E_R = 2080 \pm 50$ keV, where the resonance energy has only a minor effect on the resonance strength. We attain an upper limit of $\omega\gamma_{p_0+p_1} < 6\,\mu$eV. Assuming the ratio of the p_0 and p_1 channel to $p_{\rm tot}$ as determined by Becker *et al.* [25] (see discussion in Sec. V), the resonance strength of the proton channel becomes $\omega\gamma_{p_{\rm tot}} < 18\,\mu$eV. This result is comparable with the finding of Spillane *et al.* [28] of $\omega\gamma = 20^{+30}_{-20}\,\mu$eV from γ-ray spectroscopy.

The present data may also allow for some conclusions with respect to a hypothetical resonance at even lower energy. Under the assumption that apart from the small nonresonant contribution, all yield observed at the lowest data point, i.e., at $E = 2.0$ MeV, arises from such a resonance, an upper limit for the resonance strength can be determined. At a 90% confidence level, the upper limit for this resonance—if located at $E_R = 1.5$ MeV—is $\omega\gamma_{\rm hypothetical} < 1.5\,\mu$eV for the p_0 and p_1 channels alone. Thus, this value already exceeds the maximum prediction of Ref. [36] and no further constraints can be derived from the present work.

V. DISCUSSION

In the present experiment, the p_0 and p_1 exit channels were observed. As known from previous work, e.g., Refs. [22,25], these contributions represent only a fraction of the total S^* factor. Note that in Ref. [25] below 3.2 MeV only the p_0 and p_1 protons could be detected and the data at lower energies were corrected by adding a constant value of $S^*_{p_2,p_3,\ldots}(E) = 7.3 \times 10^{15}$ MeVb. In Fig. 6, the ratio $S_{p_0+p_1}(E)/S_{p_{\rm tot}}(E)$ from the experimental data of Becker *et al.* [25] is plotted. It is an unexpected finding that the energy dependence of this ratio reveals, on average, a linear trend with a slightly negative slope over the entire energy range. Similarly, the ratio between S^* factor of the proton channel and the total $^{12}C + ^{12}C$ S^* factor from the measurement of Becker *et al.* [25] again follows, on average, a linear trend as shown in Fig. 7. Combining the two ratios just discussed, $S_{p_0+p_1}$ contributes with a nearly constant

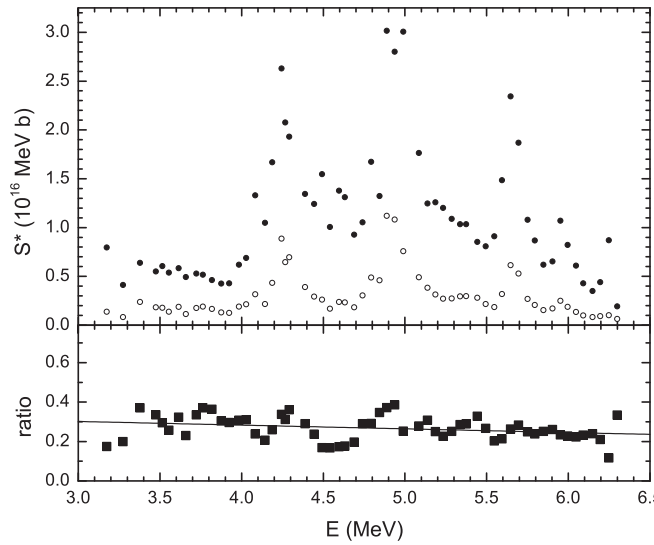

FIG. 6. The upper panel shows the modified S^* factor for the $p_{\rm tot}$ (filled circles) and $p_0 + p_1$ channel (open circles) from Ref. [25] above 3.2 MeV. The lower panel displays the ratio between the sum of these two components and the total S^* factor of the proton channel. Surprisingly, this ratio seems to be described well by a linear trend and the solid line represents a linear fit to the data. This trend was used to correct the data of the present work.

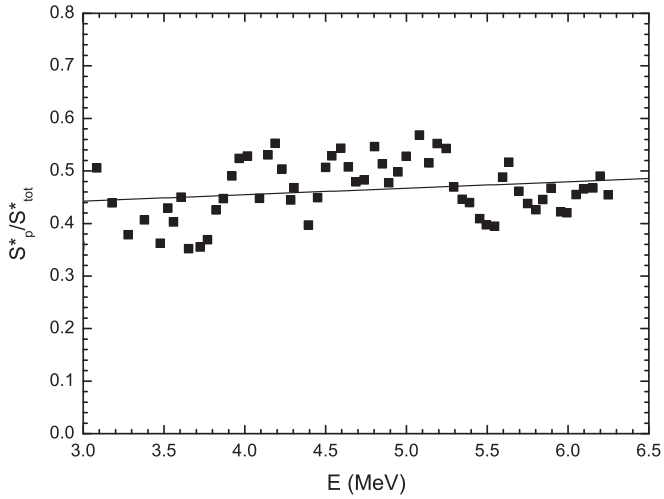

FIG. 7. The ratio between the proton-channel S^* factor and the total S^* factor, i.e., the sum of the proton and α channel, over a wide energy range from the measurement of Ref. [25]. Again, the ratio seems to be described reasonably well by a linear trend and the solid line represents a linear fit to the data.

value of approximately 14% over a wide energy range to the total $^{12}C + ^{12}C$ S^* factor. Although there is no guarantee that the observed linear trend continues toward lower energies, in particular since more channels close with decreasing energy, this ratio in the absence of more accurate information has been used in the past—including the recent work of Jiang *et al.* [29]—to correct experimental data and calculate the $^{12}C + ^{12}C$ S^* factor and the corresponding total fusion rate. However, in the light of the present results, see Fig. 5, these previous low-energy analyses and extrapolations may carry a larger uncertainty than quoted. Additionally, this approach neglects the possible influences of resonance structures which seem to be present in all channels. This ambiguity introduces further uncertainty in the presence of the large statistical uncertainties of the data below 3 MeV. Therefore, given the present status of experimental $^{12}C + ^{12}C$ data and the complexity of the system, the present data are insufficient to give a recommendation for the total S^* factor and the $^{12}C + ^{12}C$ fusion reaction rate.

VI. SUMMARY AND OUTLOOK

We have used the CIRCE 3 MV accelerator to measure protons from the $^{12}C + ^{12}C$ fusion reaction down to $E = 2.0$ MeV. This is an extension of charged particle measurements down to the upper edge of the Gamow window for this reaction. The results are in fair agreement with previous results by both γ-ray and charged-particle experiments. A low-energy resonance around 2.1 MeV which had been first observed in a previous γ-ray experiment [28] cannot be excluded by the present low-energy data. However, the large statistical uncertainties and the remaining ambiguities due to the beam-induced background make a precise determination of the resonance strength difficult, and only an upper limit can be provided.

Necessary developments that allowed these measurements to be obtained were the use of an HOPG carbon target that had very low intrinsic hydrogen content as well as a significant reduction of hydrogen isotopes in the vacuum rest gas. These improvements held interference from a two-step process starting with ^{12}C interacting with a contaminant deuterium nucleus in the carbon target to a minimum.

Extending $^{12}C + ^{12}C$ measurements to lower energy is critical as a resonance has been proposed [36] at 1.5 MeV which would have a significant impact on the reaction rates at astrophysical energies. An upper limit for the strength of such a resonance from our thick target yield was estimated and is in agreement with the theoretical work [36]. As a consequence, no further constraints can be derived from the present work.

The present work illustrates the difficulties of extrapolations of high-energy data to the relevant Gamow energy region. The experiment extends the previously achieved low-energy measurement by charged particle spectroscopy to 2 MeV, which corresponds to the high-energy side of the astrophysically relevant temperature. Present knowledge of level structures and nonresonant contribution cannot explain the results of the present experiment which may change the $^{12}C + ^{12}C$ reaction rate significantly. Further extension of charged particle and γ-ray measurements to lower energies will require an additional reduction in hydrogen contamination, increased detection efficiency, longer beam times, and targets capable of handling high beam currents. These experimental modifications are necessary to gain the statistics necessary to properly determine the resonance parameters in the vicinity of 2.1 MeV and below.

ACKNOWLEDGMENTS

The authors thank C.A. Barnes (deceased), H.-W. Becker, X. Fang, X. Tang, and F. Haas for fruitful discussions and Y. J. Guan for help during the course of the experiment. The project was supported in part by DFG (Ro429/44-1) and INFN (ERNA).

[1] E. M. Burbidge, C. R. Burbidge, W. A. Fowler, and F. Hoyle, Rev. Mod. Phys. **29**, 547 (1957).
[2] W. A. Fowler, Rev. Mod. Phys. **56**, 149 (1984).
[3] C. Rolfs and W. S. Rodney, *Cauldrons in the Cosmos* (University of Chicago Press, Chicago, 1988).
[4] S. A. Becker and I. Iben Jr., Astrophys. J. **232**, 831 (1979).
[5] C. Ritossa, E. Garcia-Berro, and J. I. Iben, Astrophys. J. **460**, 489 (1996).
[6] S. E. Woosley, A. Heger, and T. A. Weaver, Rev. Mod. Phys. **74**, 1015 (2002).
[7] F. Hoyle and W. A. Fowler, Astrophys. J. **132**, 565 (1960).
[8] I. Iben Jr. and A. V. Tutukov, Astrophys. J. Suppl. Ser. **54**, 335 (1984).
[9] A. M. Khokhlov, Astron. Astrophys. **245**, 114 (1991).
[10] E. Bravo, L. Piersanti, I. Domínguez, O. Straniero, J. Isern, and J. A. Escartin, Astron. Astrophys. **535**, A114 (2011).
[11] W. Hillebrandt and J. Niemeyer, Annu. Rev. Astron. Astrophys. **38**, 191 (2000).

[12] S. E. Woosley, S. Wunsch, and M. Kuhlen, Astrophys. J. **607**, 921 (2004).
[13] G. R. Caughlan and W. A. Fowler, At. Nucl. Data Tables **40**, 283 (1988).
[14] A. Chieffi, M. Limongi, and O. Straniero, Astrophys. J. **502**, 737 (1998).
[15] M. F. El Eid, B. Meyer, and L. The, Astrophys. J. **611**, 452 (2004).
[16] O. Straniero, L. Piersanti, and S. Cristallo, J. Phys.: Conf. Ser. **665**, 012008 (2016).
[17] G. J. Michaud and E. W. Vogt, Phys. Rev. C **5**, 350 (1972).
[18] C. L. Jiang, K. E. Rehm, B. B. Back, and R. V. F. Janssens, Phys. Rev. C **75**, 015803 (2007).
[19] M. Pignatari, R. Hirschi, M. Wiescher, R. Gallino, M. Bennett, M. Beard, C. Fryer, F. Herwig, G. Rockefeller, and F. X. Timmes, Astrophys. J. **762**, 31 (2013).
[20] J. R. Patterson, H. Winkler, and C. S. Zaidins, Astrophys. J. **157**, 367 (1969).
[21] H. Spinka and H. Winkler, Nucl. Phys. A **233**, 456 (1974).
[22] M. G. Mazarakis and W. E. Stephens, Phys. Rev. C **7**, 1280 (1973).
[23] K. U. Kettner, H. Lorenz-Wirzba, and C. Rolfs, Phys. Rev. Lett. **38**, 337 (1977).
[24] M. D. High and B. Cujec, Nucl. Phys. A **282**, 181 (1977).
[25] H. W. Becker, K. U. Kettner, C. Rolfs, and H. P. Trautvetter, Z. Phys. A **303**, 305 (1981).
[26] E. F. Aguilera, P. Rosales, E. Martinez-Quiroz, G. Murillo, M. Fernandez, H. Berdejo, D. Lizcano, A. Gomez-Camacho, R. Policroniades, A. Varela *et al.*, Phys. Rev. C **73**, 064601 (2006).
[27] L. Barron-Palos, E. F. Aguilera, J. Aspiazu, A. Huerta, E. Martinez-Quiroz, R. Monoroy, E. Moreno, G. Murillo, M. E. Ortiz, R. Policroniades *et al.*, Nucl. Phys. A **779**, 318 (2006).
[28] T. Spillane, F. Raiola, C. Rolfs, D. Schurmann, F. Strieder, S. Zeng, H.-W. Becker, C. Bordeanu, L. Gialanella, M. Romano, and J. Schweitzer, Phys. Rev. Lett. **98**, 122501 (2007).
[29] C. L. Jiang, D. Santiago-Gonzalez, S. Almaraz-Calderon, K. E. Rehm, B. B. Back, K. Auranen, M. L. Avila, A. D. Ayangeakaa, S. Bottoni, M. P. Carpenter *et al.*, Phys. Rev. C **97**, 012801(R) (2018).
[30] X. Fang, B. Bucher, A. Howard, J. J. Kolata, A. Roberts, X. D. Tang, and M. Wiescher, Nucl. Instrum. Methods Phys. Res., Sect. A **871**, 35 (2017).
[31] J. Blocki and W. J. Swiatecki, Ann. Phys. **132**, 53 (1981).
[32] A. Diaz-Torres and M. Wiescher, Phys. Rev. C **97**, 055802 (2018).
[33] E. Vogt and H. McManus, Phys. Rev. Lett. **4**, 518 (1960).
[34] R. Perez-Torres, T. L. Belyaeva, and E. F. Aguilera, Phys. At. Nucl. **69**, 1372 (2006).
[35] R. L. Cooper and N. Narayan, Astrophys. J. **629**, 422 (2005).
[36] R. L. Cooper, A. W. Steiner, and E. F. Brown, Astrophys. J. **702**, 660 (2009).
[37] J. Zickefoose, J. Schweitzer, T. Spillane, F. Strieder, H.-W. Becker, C. Rolfs, A. Di Leva, M. De Cesare, N. De Cesare, F. Terrasi, L. Gialanella, D. Schurmann, Y. Guan, G. Imbriani, and B. Limata, PoS **NICXI**, 019 (2010).
[38] J. Zickefoose, Ph.D. thesis, University of Connecticut, 2010 (unpublished).
[39] A. Antilla, J. Keinonen, M. Hautala, and I. Forsblom, Nucl. Instrum. Methods **147**, 501 (1977).
[40] S. Harissopulos, C. Chronidou, K. Spyrou, T. Paradellis, C. Rolfs, W. H. Schulte, and H. W. Becker, Eur. Phys. J. A **9**, 479 (2000).
[41] F. Terrasi, D. Rogalla, N. De Cesere, A. D'Onofrio, C. Lubritto, F. Marzaioli, I. Passariello, M. Rubino, C. Sabbarase, G. Casa, *et al.*, Nucl. Instrum. Methods Phys. Res., Sect. B **259**, 14 (2007).
[42] P. Reichart, D. Spemann, A. Hauptner, A. Bergmaier, V. Hable, R. Hertenberger, C. Greubel, A. Setzer, G. Dollinger, D. N. Jamieson, T. Butz, and P. Equinazi, Nucl. Instrum. Methods Phys. Res., Sect. B **249**, 286 (2006).
[43] C. Iliadis, *Nuclear Physics of Stars* (Wiley-VCH Verlag, Berlin, 2007).
[44] H. Andersen and J. F. Ziegler, *The Stopping and Ranges of Ions in Matter* (Pergamon, New York, 1977); J. F. Ziegler, Nucl. Instrum. Methods Phys. Res., Sect. B **219**, 1027 (2004); and SRIM, updated version 2008 [http://www.srim.org].
[45] P. R. Christensen and A. Winther, Phys. Lett. B **65**, 19 (1976).
[46] X. Fang, B. Bucher, S. Almaraz-Calderon, A. Alongi, A. D. Ayangeakaa, A. Best, G. P. A. Berg, C. Cahillane, E. Dahlstrom, R. J. deBoer, M. Freer *et al.*, J. Phys.: Conf. Ser. **420**, 012151 (2013).
[47] H. J. Assenbaum, K. Langanke, and C. Rolfs, Z. Phys. A **327**, 461 (1987).